Spin, charge, and lattice coupling in triangular and Kagomé sublattices of CoO_4 tetrahedra: $YbBaCo_4O_{7+\delta}$ ($\delta=0,1$)

A. Maignan,* V. Caignaert, D. Pelloquin, S. Hébert, and V. Pralong
Laboratoire CRISMAT, UMR 6508 CNRS ENSICAEN, 6 bd Maréchal Juin 14050 CAEN Cedex 4, France

J. Hejtmanek
Institute of Physics, Cukrovarnická 10, 162 53 Prague 6, Czech Republic

D. Khomskii
II Physikalisches Institut, Universität zu Köln, Zulpicher Str. 77, 50937 Köln, Germany
(Received 26 May 2006; revised manuscript received 10 July 2006; published 20 October 2006)

The structural and physical properties of $YbBaCo_4O_{7+\delta}$ have been studied. The polycrystalline samples of this "114" phase of composition $Yb_{0.95}BaCo_4O_{7+\delta}$ have been prepared in air. By postannealing, two samples corresponding to $\delta\sim 0$ and $\delta\sim 1$ have been obtained. The physical properties of the compound "O_7" ($\delta\sim 0$) exhibit a hysteretic transition at $T_S=160$ K–180 K as a function of T as shown by resistivity, magnetization, and thermoelectric power measurements. These measurements indicate a hole-doped electrical conduction compatible with an activated regime for the hopping of high spin Co^{3+} holes in a matrix of high spin Co^{2+}. By increasing the oxygen content, i.e., the cobalt oxidation state from 2.25 for "O_7" to 2.75 for "O_8," the signatures of this transition are suppressed. This shows that below the structural transition at T_S, the release of the magnetic frustration helps the development of antiferromagnetic order. The latter in turn creates the charge localization at T_S.

DOI: 10.1103/PhysRevB.74.165110 PACS number(s): 75.30.Et, 71.30.+h, 71.70.Gm, 72.25.Ba

I. INTRODUCTION

Recently, the cobaltites have attracted much attention due to their remarkable electronic and magnetic properties such as magnetoresistance in perovskite $La_{1-x}Sr_xCoO_3$,[1] metal insulator transition in oxygen-deficient perovskite,[2] thermoelectric properties for the layer compound Na_xCoO_2,[3] and superconductivity for its derivated hydrated form, $Na_{0.3}CoO_2$, $1.35H_2O$.[4] Interestingly, for Na_xCoO_2 containing CoO_2 layers of the CdI_2 type, the cobalt cations network is triangular and geometrical frustration has been invoked to explain the observation of an incommensurate spin density wave without long-range magnetic ordering for small x values.[5] The occurrence of geometrical frustration in the triangular lattice is also responsible for the superparamagnetism behavior reported for the hexagonal phase $Ca_3Co_2O_6$ with a magnetization showing a "1/3 plateau"[6] as also reported recently for $SrCo_6O_{11}$.[7] The latter, crystallizing in the $P6_3/mmc$ space group, exhibits a Kagomé lattice of cobalt cations. A staircaselike Kagomé lattice is also found in the compound $Co_3V_2O_8$ characterized by two magnetic phase transitions.[8] All these studies illustrate the great role played by frustration for the generation of interesting properties in cobaltites.

In that respect, the hexagonal $YBaCo_4O_7$ compound, namely 114 phase, which structure[9–11] contains CoO_4 tetrahedra sitting in alternating layers of Kagomé and triangular arrays[11] presents definite interest [Fig. 1(a)]. Recent studies of oxygen stoichiometry in this 114 phase have revealed the existence of a large oxygen nonstoichiometry going from "O_7" to "$O_{8.5}$,"[12–14] i.e., the cobalt oxidation state varying from $v_{Co}=2.25$ to $v_{Co}=3$. According to the work on $LnBaCo_4O_7$ (Ln=Lu, Yb, Tm), the "O_7" phases are characterized by structural transitions (space group $P6_3mc$ to $Cmc2$) with characteristic temperature (T_S) increasing from $T_S=165$ K (Ln=Lu) to $T_S=230$ K (Ln=Tm) as the Ln^{3+} ionic radius decreases.[15] This transition is accompanied by the marked change of electrical resistivity. The origin of this behavior is still not clear. It was argued in Ref. 16 that this transition is caused by the tendency to optimize the Ba^{2+} bonding, strongly underbound in the high temperature phase. Another suggestion is that this transition may be caused by (partial) charge ordering of Co^{2+} and Co^{3+} at the Kagomé (Co^{2+}) and triangular (Co^{3+}) sites.[15]

Magnetic structure of $YBaCo_4O_7$ was studied recently by neutron diffraction.[11,17] In Ref. 17, it was shown that this system undergoes a long-range magnetic antiferromagnetic ordering below 110 K and has a broad T region of diffuse magnetic scattering between T_N and the structural transition at 313 K. On the other hand, $YbBaCo_4O_7$ undergoes a structural transition from trigonal ($P31c$) to orthorhombic ($Pbn2_1$) above and below ~175 K with a long-range antiferromagnetic ordering below $T_N\sim 80$ K.[16] In order to have a better understanding of the phenomena occurring in these systems and to address the question of the origin of the electrical and magnetic transition, we carried out a complete study of structural and physical properties for $YbBaCo_4O_{7+\delta}$ with $\delta=0$ or $\delta=1$.

In the following, it is proposed that the structural transition at $T_S\sim 175$ K for the O_7 stoichiometry releases the magnetic frustration. Similarly to $YBaCoO_7$,[17] it is proposed that for $T_N<T<T_S$, the setting of short-range 120° antiferromagnetic correlations hinders hole carrier hopping as probed by measurements of Seebeck coefficient and resistivity. This general picture also allows us to qualitatively explain other anomalies at the structural transition.

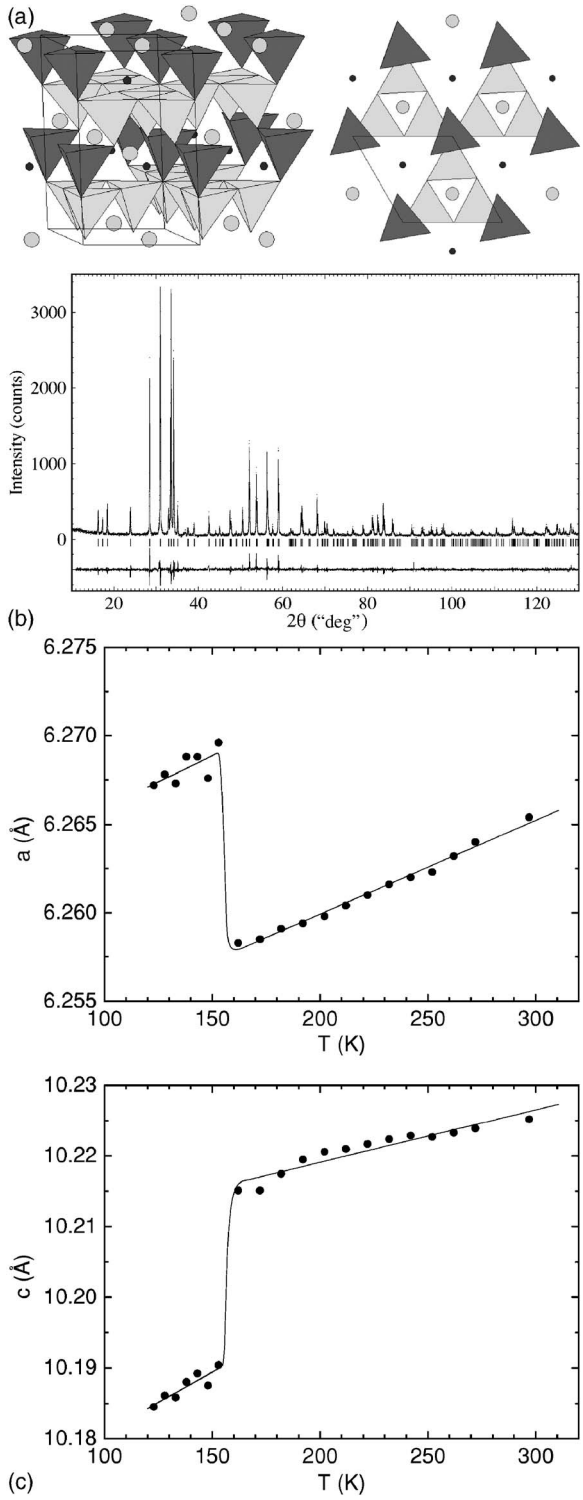

FIG. 1. (a) Perspective view of $YbBaCo_4O_7$ [left, (*ab*) plane] and projection along *c* showing the top two layers of CoO_4 tetrahedra (right). Ba^{2+} and Yb^{3+} are represented by large and small spheres, respectively. (b) Rietveld pattern of $YbBaCo_4O_7$. The difference between experimental and calculated diffraction pattern is shown at the bottom as a solid line. The row of markers shows the position of allowed reflections for space group $P6_3mc$. (c) Cell parameters evolution vs temperature.

II. SYNTHESIS AND STRUCTURAL ANALYSES

The first set of $YbBaCo_4O_{7+\delta}$ samples has been prepared by mixing stoichiometric ratios of the Yb_2O_3, $BaCO_3$, and Co_3O_4 precursors. After decarbonation at 900 °C for 12 h in air the powder was pressed in bars ($2\times2\times10$ mm). The latters were heated at 100 °C/h up to 1100 °C and after 24 h they were cooled down to room temperature in 12 h. Observations by using a JEOL 2011 FEG transmission electron microscope equipped with an energy dispersive spectroscopy (EDS) analyzer, revealed an hexagonal lattice ($a=6.3$ Å and $c=10.3$ Å) while a slight Yb^{3+} deficiency leading to the cation ratio "$Yb_{0.95}BaCo_4$" was detected. A second set was thus prepared starting from this analyzed formula. The x-ray powder diffraction (XRPD) made by a Panalytical X-pert Pro diffractometer (CuK_α, $4° \leqslant 2\theta \leqslant 120°$, $\Delta 2\theta = 0.0167°$) equipped with an Anton Paar TKK 450 (100 K–723 K) temperature chamber and an X'celerator detector, confirmed the better purity for the second run with less that 2% unreacted Co_3O_4 oxide as secondary phase. It must be emphasized that starting from the "$YbBaCo_4$" cation composition, it was not possible to avoid the formation of impurities whatever the reaction temperature and duration were.

A Rietveld analysis from the XPRD data recorded at room temperature was carried out with the Fullprof program [Fig. 1(b)]. These refinements confirm the hexagonal structural model proposed by Valldor and Anderson.[9] A similar result is observed considering the lower $P31c$ symmetry proposed by Huq *et al.*,[16] showing that from x-ray diffraction it is not possible to discriminate between these models. The cell parameters evolution as a function of temperature has been studied from 100 K to 293 K. This work performed within the hexagonal ($a\approx6.3$ Å and $c\approx10.3$ Å) $P6_3mc$ space group is summarized in Fig. 1(c). Clearly a structural transition is observed at $T_S\approx170$ K in good agreement with the previous results already published.[15,16]

The determination of the oxygen stoichiometry by both thermogravimetry under Ar/H_2 flow and iodometric titration leads to $O_{7.06(2)}$ for the as-prepared sample taking into account the "$Yb_{0.95}BaCo_4$" cation stoichiometry. According to several previous reports,[12–14] the oxygen stoichiometry of the 114 structure can be varied from O_7 to $O_{8.5}$. Consequently, the as-prepared compound was postannealed in oxygen pressure ($PO_2=10$ MPa) at 300 °C for 12 h or reduced by using an Ar flow in a thermogravimetric analysis (TGA) balance. The determination of the oxygen content in $YbBaCo_4O_{7+\delta}$ yields "$O_{7.93(2)}$" for the oxygen pressure treatment and "$O_{6.94(2)}$" for the reduced sample. For sake of clarity, in the following, these reduced and oxygenated samples are labeled $YbBaCo_4O_7$ and $YbBaCo_4O_8$, respectively. Furthermore, in order to check for a possible change of oxygen stoichiometry during the electrical resistivity and Seebeck coefficient measurements performed in air up to ~800 K, thermogravimetric analysis was also made in $PO_2=0.2$ atm. for both samples "O_7" and "O_8." They clearly show that in these conditions no loss nor uptake oxygen can be detected.

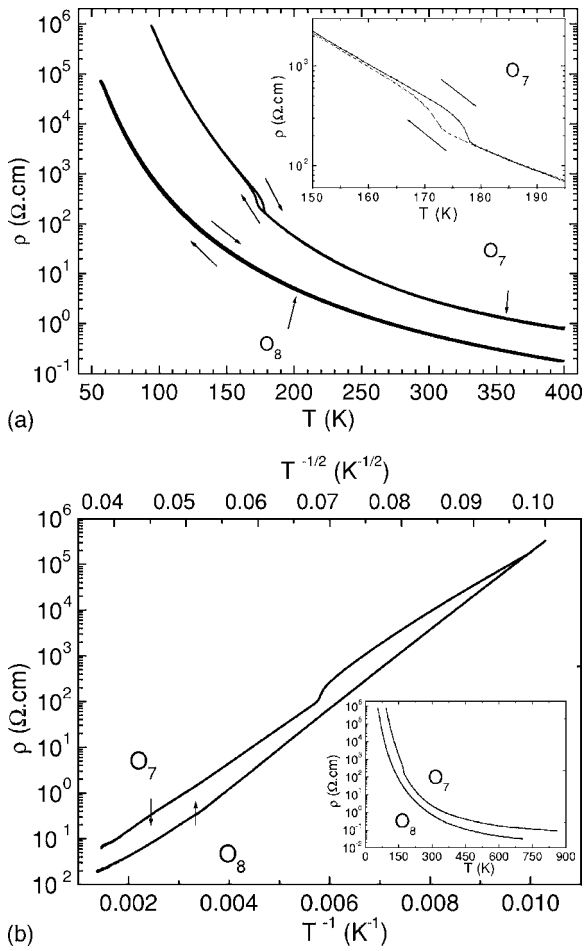

FIG. 2. (a) T-dependence resistivity ρ for $YbBaCo_4O_7$ (O_7) and $YbBaCo_4O_8$ (O_8). The arrows indicate the warming or cooling processes. Inset: enlargement of the transition observed for $YbBaCo_4O_7$. (b) $\rho(T^{-1})$ and $\rho(T^{-1/2})$ for the compounds O_7 (lower x axis) and O_8 (upper x axis), respectively. Inset: measurements collected up to 800 K.

III. ELECTRIC AND MAGNETIC PROPERTIES VERSUS OXYGEN STOICHIOMETRY

Temperature dependence of the resistivity (ρ) was measured by the four-probe technique, upon cooling and then warming. The $\rho(T)$ dependence, shown in Fig. 2(a), is characterized by negative coefficient $(d\rho/dT)<0$. At room temperature (RT), the ρ value for the sample "O_7," $\rho_{300\ K}\sim 2\ \Omega$ cm, is larger than that of O_8. More importantly, it is found that the oxygen stoichiometric sample "O_7" exhibits a hysteretic transition at 173 K (178 K) upon cooling (warming) which is enlarged in the inset of Fig. 2(a). In contrast, for the O_8 compound, this transition is suppressed with a resistivity value lower by a factor of three at 300 K. The $\rho(T^{-1})$ corresponding curve shows that the O_7 composition is semiconducting with an activation energy $E_A=155$ meV on each T side of the transition [Fig. 2(b)]. In contrast, the O_8 compound does not obey an Arrhenius law but rather the variable range hopping (VRH). These different conduction regimes are confirmed by measurements collected up to ~800 K as shown in the inset Fig. 2(b).

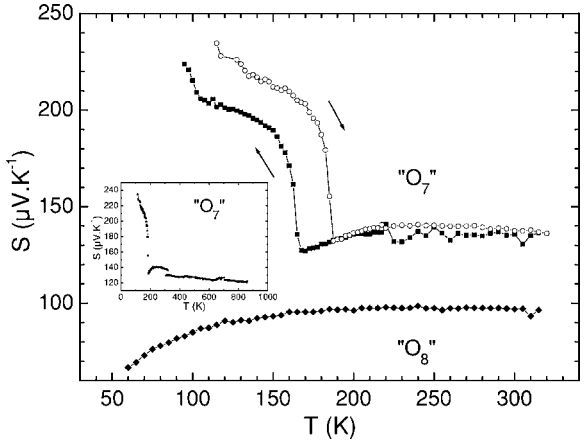

FIG. 3. T-dependent Seebeck coefficient (S) of $YbBaCo_4O_7$ (O_7) and $YbBaCo_4O_8$ (O_8). The arrows indicate data collected on cooling or warming. A clear hysteretic transition is obtained for O_7. Inset: data collected for the O_7 sample upon warming up to 850 K.

In order to probe the distinct transport mechanisms for the O_7 and O_8 samples, thermoelectric power (S) coefficient measurements have been made. As shown in Fig. 3, the $S(T)$ curves collected upon cooling show for the sample O_7, a clear jump from $S\sim 130\ \mu V\ K^{-1}$ up to $S\sim 190\ \mu V\ K^{-1}$ below 165 K, i.e., as the sample becomes less conducting due to the structural transition existing at that temperature.[15,16] This transition probed by S measurements (steady-state method) is also hysteretic with $\Delta T\sim 25$ K. This T difference is larger than that found for the resistivity measurements ($\Delta T=5$ K). This reflects the very different timescale used for these techniques with ρ measurements collected by sweeping T by 1 K min^{-1} whereas each S datum is collected after T stabilization for 30 min. This clearly demonstrates that the kinetics of the transition depends strongly on the experimental procedure. The evolution of the thermoelectric power cannot be measured below ~100 K, the resistance of the sample becoming too large. In contrast, the S (T) curve for the oxygenated compound O_8 shows a continuous decrease as T decreases without any transition down to 50 K. This behavior is in perfect agreement with the electrical resistivity showing a different transport mechanism. The $S_{300\ K}$ value of $\sim 100\ \mu V\ K^{-1}$, smaller than for the O_7 compound, agrees with the fact that the mobile-hole carrier concentration is increased by the oxygen uptake explaining the lower resistivity values. Finally we must point out that the S values, measured in air, remain almost constant at least up to 850 K as shown in the inset of Fig. 3 with $S\sim 120\ \mu V\ K^{-1}$ for $YbBaCo_4O_7$. This is a clear indication that the same transport mechanism holds above the transition.

At the structural transition temperature, detected on the $\rho(T)$ and $S(T)$ curves, a small jump is also measured on the temperature dependent magnetization (M) curves [superconducting quantum interference device (SQUID) magnetometer]. By collecting M data in field cooling mode in 0.3 T, both upon cooling (fcc) and then warming (fcw), a transition is observed at ~160 K and ~180 K for the former and the latter curves, respectively (inset of Fig. 4). This hysteretic magnetic transition is in good coincidence with the tempera-

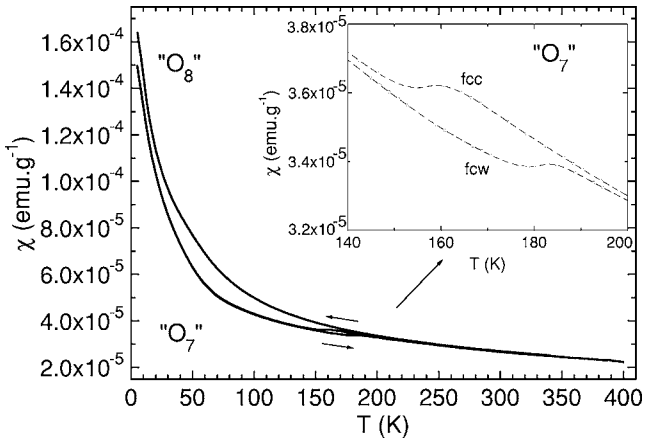

FIG. 4. T-dependent magnetization curves of $YbBaCo_4O_7$ (O_7) and $YbBaCo_4O_8$ (O_8) registered in field cooling cooling (fcc) and field cooling warming (fcw) processes as indicated by the arrows. Inset: the curves for $YbBaCoO_7$ are enlarged for T near the transition.

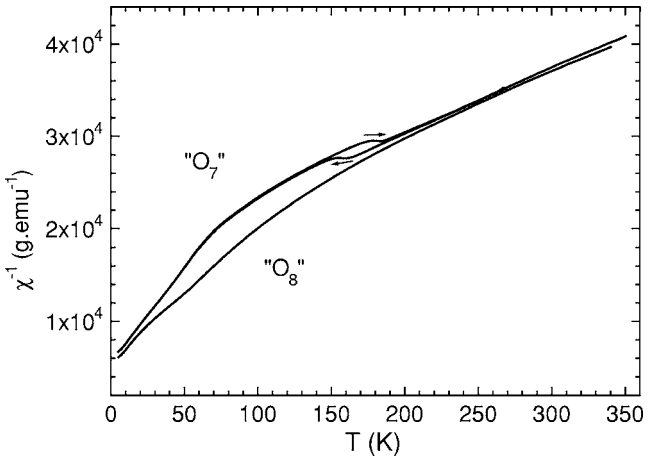

FIG. 5. T-dependent reciprocal magnetic susceptibility ($\chi=M/H$) for the $YbBaCo_4O_7$ (O_7) and $YbBaCo_4O_8$ (O_8).

ture of the electrical and Seebeck transitions [Fig. 3 and inset of Fig. 2(a)]. Starting from the high T part (400 K) of the $M(T)$ curve, the transition corresponds to a M decrease as T decreases. This is consistent with the observations of the setting of a short-range 120° antiferromagnetic ordering.[11,16] In the latter references, a clear structural transition [at $T_S=105$ K for Y (Ref. 11) and at $T_S=175$ K for Yb (Ref. 16)] corresponds to the threshold temperature of this ordering. It is thus logical to associate the change of magnetic and transport properties at T_S with the setting of antiferromagnetic order. The comparison of the $M(T)$ curves for the O_7 and O_8 samples shows that this transition is suppressed in the oxygen rich phase (Fig. 4). This fact unveils the sensitivity of this transition to the exact oxygen content, which is in direct correlation with cobalt valency.

All these sets of data support a strong interplay between the charges, the spins, and the lattice. In the low T crystallographic phase ($T<T_S$) obtained for the O_7 compound, the cobalt triangles of the two different sublattices become unequal.[11,16] Accordingly, the geometrical frustration of the cobalt network is partly released allowing a short-range 120° antiferromagnetic structure to develop, e.g., with stronger spin correlations on smaller triangles. In contrast, for the more oxidized compound (O_8), the extra oxygen tend to increase locally the coordination of the cobalt cations with formal oxidation state $Co^{2.75+}$, which in turn creates a more disordered local crystallographic structure not compatible with a cobalt magnetic ordering.

Taking into account the magnetic frustration release at the structural transition, one has to explain the concomitant electrical transition. In order to do so, the cobalt spin states must be discussed. From the paramagnetic Curie-Weiss fitting well above T_S for $YbBaCo_4O_7$ (Fig. 5), the effective paramagnetic moment $\mu_{eff}=3.8\ \mu_B$ per cobalt is obtained after substraction of the value $\mu_{eff}=4.54$ for Yb^{3+}. The $\mu_{eff}=3.8\mu_B$/Co value yields an average spin number $S=3/2$ for the cobalt cations.

At that point, the Seebeck coefficient measurements can be used to select between two different models for the transport mechanism in the O_7 sample. As shown in Figs. 6(a) and 6(b), removing an electron in the orbitals of a high spin (HS) Co^{2+}, yields a hole as either a HS Co^{3+} [Fig. 6(a)] or an intermediate spin (IS) Co^{3+} [Fig. 6(b)].[18] In order to respect the formal mixed valency, $v_{Co}=2.25$, one obtains thus either

$$\frac{Co^{3+}(HS)}{Co^{2+}(HS)}=\frac{1}{3} \quad \text{or} \quad \frac{Co^{3+}(IS)}{Co^{2+}(HS)}=\frac{1}{3},$$

for which one expects $\mu_{eff}=4.13\ \mu_B$/Co and $\mu_{eff}=3.61\ \mu_B$/Co, respectively. As the experimental value is intermediate $\mu_{eff}=3.8\ \mu_B$/Co, one has to calculate the Seebeck coefficient values for the situations corresponding to Figs. 6(a) and 6(b). In the high T limit, the Heikes formula is written

$$S=-\frac{k_B}{e}\ln\left(\beta\frac{x}{1-x}\right), \tag{1}$$

where $x=\frac{1}{4}$ is the theoretical Co^{3+} hole concentration and β the spin degeneracy term, $\beta=(2S+1)^{Co^{2+}}/(2S+1)^{Co^{3+}}$ (Ref. 19). By considering a mixture of HS Co^{2+}/Co^{3+} [Fig. 6(a)], one obtains $\beta=\frac{4}{5}$ and thus $S_{T\to\infty}=114\ \mu V\ K^{-1}$, whereas for the mixture of HS Co^{2+} and IS Co^{3+} one obtains $\beta=\frac{4}{3}$, from which one would obtain $S_{T\to\infty}=70\ \mu V\ K^{-1}$. When compared to the experimental data (inset of Fig. 3), $S_{800\ K}$

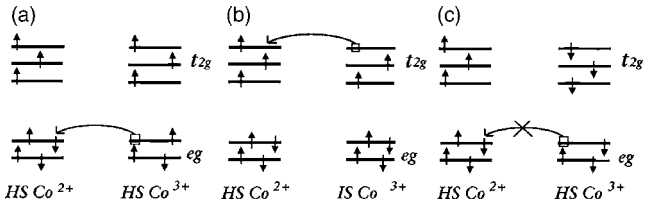

FIG. 6. Drawing of the t_{2g} and e_g orbitals for Co^{2+} and Co^{3+} in the CoO_4 tetrahedral configuration. (a) Hole hopping in the e_g orbitals between high spin Co^{3+} to Co^{2+} (curved arrow). (b) Hole hopping in the t_{2g} orbitals between two neighboring cobalt cations, intermediate spin Co^{3+} and high spin Co^{2+}. (c) If the t_{2g} spins of the neighboring cobalt are antiparallel, the hole hopping described in (a) requires a spin flip.

$=120\ \mu V\ K^{-1}$, the first scenario involving a mixture of HS Co^{2+}/Co^{3+} gives a much better agreement.

From the large S increase below the transition temperature to $S\sim 190\ \mu V\ K^{-1}$, from Eq. (1), one can also derive another fraction of Co^{3+} $x=0.12$ instead of $x=0.25$. Roughly, below the transition, it is as if half of the mobile holes become localized.

Now, comparing the drawing [Fig. 6(a)], it is obvious that the hopping in the e_g orbitals is "easier" between ferromagnetically polarized adjacent cobalt cations than in case of antiferromagnetic interaction [Fig. 6(c)], where the spin "flip" is necessary (this situation is similar to the usual double exchange). As a consequence, as the nearest-neighbor antiferromagnetic interaction is strengthened below the structural transition temperature T_S, a part of hopping electrons "becomes" trapped, leading to the increase of thermoelectric power.

On the other hand, the lower S values observed for the more oxidized O_8 compound results from the increase of the Co^{3+} content. The quantitative assessment of the thermoelectric power using the simple configuration and spin entropy picture adopting the same starting platform as for O_7 compound, i.e., the high spin state of both Co^{2+} and Co^{3+}, however, fails. Most importantly, in the simple ionic picture of the strongly correlated systems, one should expect not positive but negative thermopower, since in this case we have one Co^{2+} per three Co^{3+}, i.e., charge carriers would be Co^{2+} electrons. But the observation of a positive thermopower of about $100\ \mu V\ K^{-1}$ could indicate that the charge carriers in the O_8 phase behave more like itinerant ones in a sense of band picture: one would have more than half-filled e_g band for both O_7 and O_8 samples, leading to a holelike conduction and positive thermopower in both cases. This conclusion agrees perfectly with the smaller resistivity of the O_8 sample [Fig. 2(a)]. It also agrees with the VRH nature of the O_8 sample conductivity, implying "itinerant" electron states with the "apparent" insulating behavior due to magnetic frustration (or Anderson localization).

IV. CONCLUSIONS

It is argued that it is the setting of antiferromagnetic correlations at the structural transition in the hole-doped $YbBaCo_4O_7$ compounds which can be responsible for the anomalous properties of the 114 compounds. By increasing the hole concentration in the "$O_{7+\delta}$" phase, the extra oxygens hinder the triangular arrangement for the magnetic moments of the tetrahedrally coordinated CoO_4 since new polyhedra are created. This suppresses the magnetostrictive transition. On the other hand, oxygen-rich samples seem to behave in a more itinerant manner. The oxygen stoichiometry is thus a crucial parameter governing the properties of the $RBaCo_4O_{7+\delta}$ systems.

*Corresponding author. Present address: Laboratoire CRISMAT, UMR 6508, CNRS/ENSICAEN, 6 bd du Maréchal Juin, 14050 CAEN Cedex 4-France. Email address: antoine.maignan@ensicaen.fr

[1] S. Yamaguchi, H. Taniguchi, H. Takagi, T. Arima, and Y. Tokura, J. Phys. Soc. Jpn. **64**, 1885 (1995).
[2] D. Akahoshi and Y. Ueda, J. Phys. Soc. Jpn. **68**, 736 (1999).
[3] I. Terasaki, Y. Sasago, and K. Uchinokura, Phys. Rev. B **56**, R12685 (1997).
[4] K. Takada, H. Sakurai, E. Takayama-Muromachi, F. Izumi, R. A. Dilanian, and T. Sasaki, Nature (London) **422**, 53 (2003).
[5] J. Sugiyama, J. H. Brewer, E. J. Ansaldo, H. Itahara, T. Tani, M. Mikami, Y. Mori, T. Sasaki, S. Hébert, and A. Maignan, Phys. Rev. Lett. **92**, 017602 (2004).
[6] A. Maignan, C. Michel, A. C. Masset, C. Martin, and B. Raveau, Eur. J. Phys. B **5**, 657 (2000).
[7] S. Ishiwata, D. Wang, T. Saito, and M. Takano, Chem. Mater. **17**, 2789 (2005).
[8] N. Rogado, G. Lawes, D. A. Huse, A. P. Ramirez, and R. J. Cava, Solid State Commun. **124**, 229 (2002).
[9] M. Valldor and M. Anderson, Solid State Sci. **4**, 923 (2002).
[10] M. Valldor, Solid State Sci. **6**, 251 (2004).
[11] M. Soda, Y. Yasui, T. Moyoshi, M. Sato, N. Igawa, and K. Kakurai, J. Phys. Soc. Jpn. **75**, 054707 (2006).
[12] E. V. Tsipis, V. V. Kharton, J. R. Frade, and P. Nunez, J. Solid State Electrochem. **9**, 547 (2005).
[13] E. V. Tsipis, D. D. Khalyavin, S. V. Shiryaev, K. S. Redkina, and P. Nunez, Mater. Chem. Phys. **92**, 33 (2005).
[14] M. Karppinen, H. Yamauchi, S. Otami, T. Fujita, T. Motohashi, Y. H. Huang, M. Valkeapää, and H. Fjellag, Chem. Mater. **18**, 490 (2006).
[15] N. Nakayama, T. Mizota, Y. Ueda, A. N. Sokolov, and A. N. N. Vasiliev, J. Magn. Magn. Mater. **300**, 98 (2006).
[16] A. Huq, J. F. Mitchell, H. Zheng, L. C. Chapon, P. G. Radaelli, K. S. Knight, and P. W. Stephens, J. Solid State Chem. **179**, 1136 (2006).
[17] L. C. Chapon, P. G. Radaelli, H. Zheng, and J. F. Mitchell, cond-mat/0605307 (unpublished).
[18] Note: for a regular tetrahedral coordination, both intermediate spin (IS) and low spin (LS) states of Co^{3+} coincide ($e_g^4 t_{2g}^2$, $S=1$). In the text, the terminology IS is used by analogy with Co^{3+} in octahedra, where the $S=1$ state is an IS state, and also to avoid misunderstanding as usually the LS notation is used for the nonmagnetic ($S=0$) Co^{3+} state.
[19] J. P. Doumerc, J. Solid State Chem. **110**, 419 (1994).